Editors' Suggestion | Featured in Physics

Superconductivity in Uniquely Strained RuO_2 Films

Masaki Uchida,[1,2,3,*] Takuya Nomoto,[1] Maki Musashi,[1,2] Ryotaro Arita,[1,4] and Masashi Kawasaki[1,2,4]
[1]Department of Applied Physics, University of Tokyo, Tokyo 113-8656, Japan
[2]Quantum-Phase Electronics Center (QPEC), University of Tokyo, Tokyo 113-8656, Japan
[3]PRESTO, Japan Science and Technology Agency (JST), Tokyo 102-0076, Japan
[4]RIKEN Center for Emergent Matter Science (CEMS), Wako 351-0198, Japan

(Received 5 May 2020; accepted 27 August 2020; published 29 September 2020)

We report on strain engineering of superconductivity in RuO_2 single-crystal films, which are epitaxially grown on rutile TiO_2 and MgF_2 substrates with various crystal orientations. Systematic mappings between the superconducting transition temperature and the lattice parameters reveal that shortening of specific ruthenium–oxygen bonds is a common feature among the superconducting RuO_2 films. *Ab initio* calculations of electronic and phononic structures for the strained RuO_2 films suggest the importance of soft phonon modes for emergence of the superconductivity. The findings indicate that simple transition metal oxides such as those with a rutile structure may be suitable for further exploring superconductivity by controlling phonon modes through the epitaxial strain.

DOI: 10.1103/PhysRevLett.125.147001

Transition metal oxides represented by cuprates and ruthenates have guided us to a better understanding of unconventional superconductivity originating in strong electron correlation [1]. In some other oxides such as titanates, on the other hand, it has been thought that lattice vibrations or phonons play a more dominant role for pairing electrons in the superconducting state. In this context, binary oxide superconductors including Ti_nO_{2n-1} ($n = 1$–4) [2–7], NbO [3], SnO [8], and LaO [9] are intriguing systems. Many of them have been realized only in epitaxial films, and their superconducting mechanisms are still elusive. In these films, epitaxial strain which directly tunes lattice parameters is expected to be useful for designing superconductivity by controlling phonon modes, electron correlation, and so on, as recently demonstrated in $SrTiO_3$ thin films [10,11].

RuO_2 with a rutile structure is well known to be a highly conducting binary oxide [12,13]. RuO_2 finds many engineering applications in electrodes, thermometers, and also catalysts, and thin films, mostly polycrystalline films, have been prepared for such purposes by various growth methods [14–24]. In recent years, on the other hand, RuO_2 has attracted renewed attention as a high-temperature antiferromagnet [25,26] and a possible topological nodal line semimetal [27,28], demanding a reexamination of its electronic transport in the ground state. It has been also reported that superconductivity appears in RuO_2 thin films grown on a rutile TiO_2 substrate [29]. Motivated by this, here we systematically investigate the epitaxial strain effect on superconductivity in RuO_2 films.

RuO_2 thin films were grown on single-crystal rutile TiO_2 and MgF_2 substrates with various crystal orientations in an oxide molecular beam epitaxy system [30–32], by which we are referring to molecular beam epitaxy of IrO_2 with the same rutile structure and similar volatile binary phases [33,34]. 3 nines 5 Ru elemental flux was supplied from an electron beam evaporator. Optimized growth was performed at a substrate temperature of 300 °C, regulated with a semiconductor-laser heating system, and with flowing pure O_3 with a pressure of 6×10^{-7} torr, supplied from a Meidensha ozone generator. The film thickness was adjusted in the range 26–32 nm to effectively apply large epitaxial strain. Longitudinal resistivity was measured with a standard four-probe method in a Quantum Design PPMS cryostat equipped with a 9 T superconducting magnet and a ^{3}He refrigerator. Density functional theory calculations were performed by using the Quantum Espresso package [35]. The exchange correlation functional proposed by Perdew *et al.* [36] and pseudopotentials by Garrity *et al.* [37] were used in the calculations. Phonon band structures were obtained by using density functional perturbation theory [38]. The $12 \times 12 \times 12$ k points and $3 \times 3 \times 3$ q points were used for the electronic structure calculations and the dynamical matrix calculations, respectively.

Figure 1(a) shows x-ray diffraction (XRD) θ-2θ scan of a RuO_2 thin film grown on the (110)-oriented TiO_2 substrate (sample A). It shows only sharp ($ll0$) RuO_2 peaks (l: integer) nearby the substrate ones, indicating that single-crystal RuO_2 is epitaxially grown on the substrate with the same rutile structure. As confirmed in Fig. 1(b), longitudinal resistivity of sample A begins to drop at $T_{c,\mathrm{onset}} = 1.8$ K, decreases by half at $T_{c,\mathrm{mid}} = 1.7$ K, and then becomes zero at $T_{c,\mathrm{zero}} = 1.6$ K . Increasing the out-of-plane magnetic field up to 12 000 Oe, the superconducting transition gradually shifts to lower temperatures and

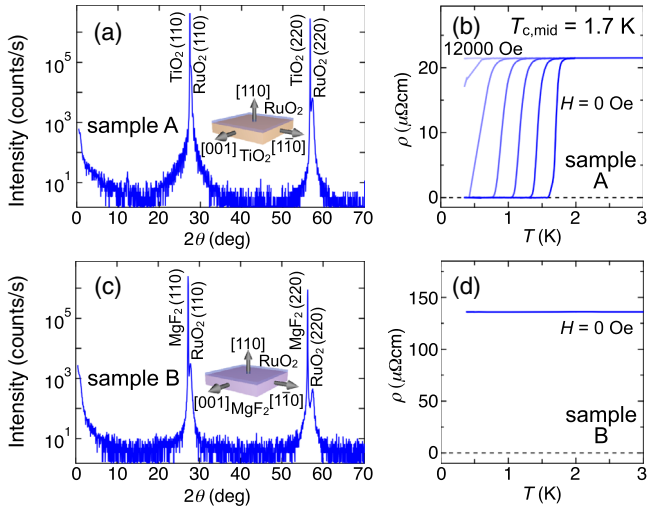

FIG. 1. Superconducting and nonsuperconducting RuO_2 thin films. (a) XRD θ–2θ scan of sample A, which is a RuO_2 film grown on the (110)-oriented TiO_2 substrate. (b) Temperature dependence of the in-plane resistivity for sample A, measured by applying a magnetic field parallel to the out-of-plane direction at intervals of 2000 Oe. It shows a clear superconducting transition with a midpoint temperature of $T_{c,\mathrm{mid}} = 1.7$ K. (c) XRD scan of sample B, a RuO_2 film grown on the (110)-oriented MgF_2 substrate. (d) Low-temperature resistivity of sample B down to 0.4 K.

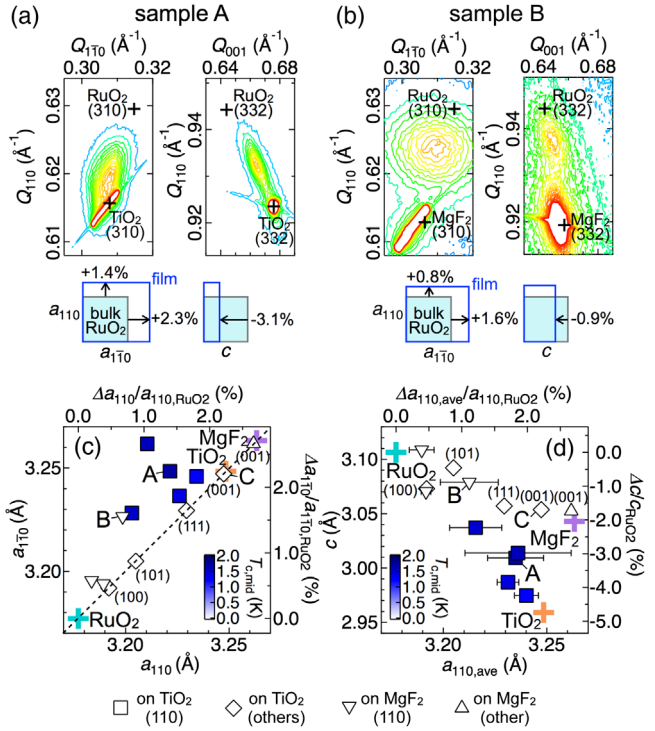

FIG. 2. Superconductivity in uniquely strained RuO_2 films. (a), (b) XRD reciprocal space mappings in samples A and B, taken for asymmetric reflections in both the $(1\bar{1}0)$ and (001) in-plane directions. The cross denotes peak positions calculated from bulk lattice parameters of RuO_2, TiO_2, and MgF_2. Changes in the RuO_2 lattice parameters from the bulk values are also schematically illustrated. (c) Mapping of the lattice parameters a_{110} vs $a_{1\bar{1}0}$ measured for all the samples grown on TiO_2 or MgF_2 substrates with different crystal orientations, as shown near the symbols. This includes sample C, grown on the (001)-oriented TiO_2 substrate. The symbol color indicates the midpoint superconducting transition temperature. (d) Mapping of $a_{110,\mathrm{ave}}$ vs c, also color coded to indicate the superconducting transition temperature. $a_{110,\mathrm{ave}}$ signifies the average of a_{110} and $a_{1\bar{1}0}$, which are shown as both ends of the horizontal bar appended for the case of the anisotropic strain. A cross indicates bulk lattice parameters of RuO_2, TiO_2, and MgF_2.

eventually disappears. This is in contrast to the other ruthenate superconductor Sr_2RuO_4 [39], in which the out-of-plane upper critical field is much lower (750 Oe in bulks and 2200 Oe in thin films), while the transition temperature is comparable [31,40].

Another RuO_2 film on the (110)-oriented MgF_2 substrate (sample B) is also epitaxially grown in the single-crystal form, as shown in Fig. 1(c). In Fig. 1(d), on the other hand, sample B does not exhibit the superconducting transition down to 0.4 K. This suggests the importance of elaborate strain engineering for the emergence of superconductivity in RuO_2. Possibly due to misfit dislocations stemming from the lattice mismatched heterointerfaces, residual resistivity of these samples is much higher than the values of about 0.05 to 2 $\mu\Omega$ cm reported in RuO_2 bulks [12,13]. On the other hand, there is no definite correlation between the residual resistivity and the emergence of superconductivity among all the samples discussed below [41].

Reciprocal space mappings in Figs. 2(a) and 2(b) demonstrate how the epitaxial strain affects film lattice parameters a_{110}, $a_{1\bar{1}0}$, and c, which are along three directions [(110), $(1\bar{1}0)$, and (001)] orthogonal to each other. In sample A, the film lattice is coherently grown and fully strained by $+2.3\%$ in a complete match with the substrate lattice along the in-plane $(1\bar{1}0)$ direction, while it is partially strained and the substrate one along the other does not match in the in-plane (001) direction. In sample B, on the other hand, the lattice is partially strained for both the $(1\bar{1}0)$ and (001) directions by $+1.6\%$ and -0.9%. Namely, while a_{110} and $a_{1\bar{1}0}$ are anisotropically extended in both the (110)-oriented films, c is greatly shortened in sample A compared to sample B, reflecting the large c-axis mismatch of -4.7% between TiO_2 and RuO_2.

Figures 2(c) and 2(d) summarize the three lattice parameters a_{110}, $a_{1\bar{1}0}$, and c measured for all the samples including other orientation films, with a comparison of their changes to the RuO_2, TiO_2, and MgF_2 bulks. For example, a film grown on the (001)-oriented TiO_2 substrate (sample C) is fully strained along the in-plane (110) and $(1\bar{1}0)$ directions, as confirmed in Fig. 2(c). This is also the case on the (001)-oriented MgF_2 substrate. Actually, except for the (110)-oriented films such as samples A and B, a_{110} and $a_{1\bar{1}0}$ are isotropically extended in all of the films. Aside from as

such isotropically strained films, no superconductivity appears even in the (110)-oriented films on MgF_2, although the a_{110} and $a_{1\bar{1}0}$ values (especially those of sample B) are nearly equal to the ones of the (110)-oriented superconducting films on TiO_2. Rather, correlation between the superconductivity and the epitaxial strain is clearly visualized in the mapping for the c-axis change in Fig. 2(d). The superconductivity emerges only in the (110)-oriented RuO_2 films grown on TiO_2, where c is shortened by 2% or much more, unlike the other films.

Rutile oxides can be roughly categorized into two types, by the magnitude relation between two metal (M)–oxygen (O) bond lengths $a_{M\text{–O}(1)}$ and $a_{M\text{–O}(2)}$, as illustrated in Figs. 3(a) and 3(b). In the RuO_2 bulk with a $M-\mathrm{O}(2)$ bond longer than the $M-\mathrm{O}(1)$ one, the d_{xy} state has slightly lower energy and is fully occupied by the $4d$ electrons, while the d_{yz}/d_{zx} states are half filled. In the TiO_2 bulk, on the other hand, the $M-\mathrm{O}(1)$ bond length is longer than the $M-\mathrm{O}(2)$ one, and thus the energy splitting

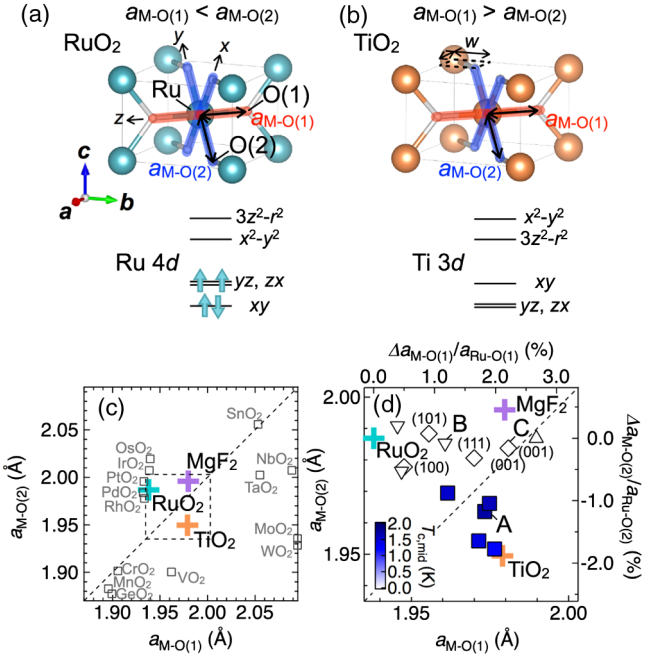

FIG. 3. Two types of the rutile structure. (a) Rutile crystal structure of bulk RuO_2, composed of short $M-\mathrm{O}(1)$ and long $M-\mathrm{O}(2)$ bonds. Simple configuration of the $4d^4$ electrons determined by the resultant crystal field splitting is also shown. (b) Case of TiO_2, where the $M-\mathrm{O}(1)$ [$M-\mathrm{O}(2)$] bonds are inversely extended [shortened] and the energy splittings within the t_{2g} and e_g levels are also reversed. (c) Mapping of the two bond lengths $a_{M\text{–O}(1)}$ vs $a_{M\text{–O}(2)}$, calculated from the lattice parameters a and c and the Wyckoff position coordinate w for many rutile compounds. (d) $a_{M\text{–O}(1)}$ vs $a_{M\text{–O}(2)}$ similarly estimated for all the RuO_2 film samples, plotted on a magnified area corresponding to the dashed box in (c). Here the average is plotted for anisotropic cases where a_{110} and $a_{1\bar{1}0}$ have different values. The symbols are colored by the superconducting transition temperature as in Figs. 2(c) and 2(d).

between the d_{xy} and d_{yz}/d_{zx} states is expected to be reversed. $a_{M\text{–O}(1)}$ and $a_{M\text{–O}(2)}$ can be calculated from the lattice parameters a and c and the Wyckoff position coordinate w using the following relations:

$$a_{M\text{–O}(1)} = \sqrt{2}wa, \tag{1}$$

$$a_{M\text{–O}(2)} = \sqrt{[\sqrt{2}(0.5-w)a]^2 + (c/2)^2}. \tag{2}$$

Here $w = 0.305$ is used for film samples because w is almost independent of the compounds and in the range 0.3045–0.3065. As confirmed in Fig. 3(c), RuO_2 and TiO_2 are located in the regions $a_{M\text{–O}(1)} < a_{M\text{–O}(2)}$ and $a_{M\text{–O}(1)} > a_{M\text{–O}(2)}$, respectively, while averages of $a_{M\text{–O}(1)}$ and $a_{M\text{–O}(2)}$ are almost the same. MgF_2, which has near-TiO_2 $a_{M\text{–O}(1)}$ and near-RuO_2 $a_{M\text{–O}(2)}$, is rather close to the region boundary. Figure 3(d) reveals an important trend of $a_{M\text{–O}(1)}$ vs $a_{M\text{–O}(2)}$, which distinguishes the superconducting and nonsuperconducting RuO_2 films. Namely, in the superconducting films (e.g., sample A), $a_{M\text{–O}(2)}$ substantially decreases as the TiO_2 bulk value is approached, in addition to the increase of $a_{M\text{–O}(1)}$. On the other hand, only the increase of $a_{M\text{–O}(1)}$ is confirmed in the nonsuperconducting films (e.g., samples B and C), whose parameters are distributed between the RuO_2 and MgF_2 bulks. This map clearly indicates that the shortening of the $M-\mathrm{O}(2)$ bonds is essential for emergence of the superconductivity.

Next we examine strain effects on fundamental electronic and phononic properties in RuO_2. Figure 4(a) compares the electron density of states between the RuO_2 bulk and strained thin films (samples A, B, and C). The density of states ranging between $E-E_F \sim -1.5$ and 1.2 eV is mainly from the Ru t_{2g} bands and the bulk band structure is consistent with previous calculations [42]. In the film samples with the extended $M-\mathrm{O}(1)$ and shortened $M-\mathrm{O}(2)$ bonds or even only with the extended $M-\mathrm{O}(1)$ bonds, it is expected that the d_{xy} band is relatively shifted to higher energies. However, a peak at $E-E_F \sim -0.5$ eV ascribed to the d_{xy} band, for example, is shifted only about 0.2 eV even in superconducting sample A, which is small compared to the bandwidth. In particular, the calculated density of states at the Fermi level is not substantially different among the superconducting and nonsuperconducting samples.

In contrast, phonon dispersion relations are largely modulated by the lattice parameter change. As shown in Fig. 4(b), two specific phonon modes in superconducting sample A exhibit negative frequencies indicating dynamical instability. Nearly degenerate modes originally with the lowest energies along the $\Gamma-Z$ line, which are the acoustic modes oscillating on the $a-b$ plane (modes 1 and 2), remain almost unchanged. On the other hand, phonon softening occurs in the one with the second lowest energy, which is the acoustic mode oscillating along the c direction (mode 3). Similar softening also occurs in the optical mode

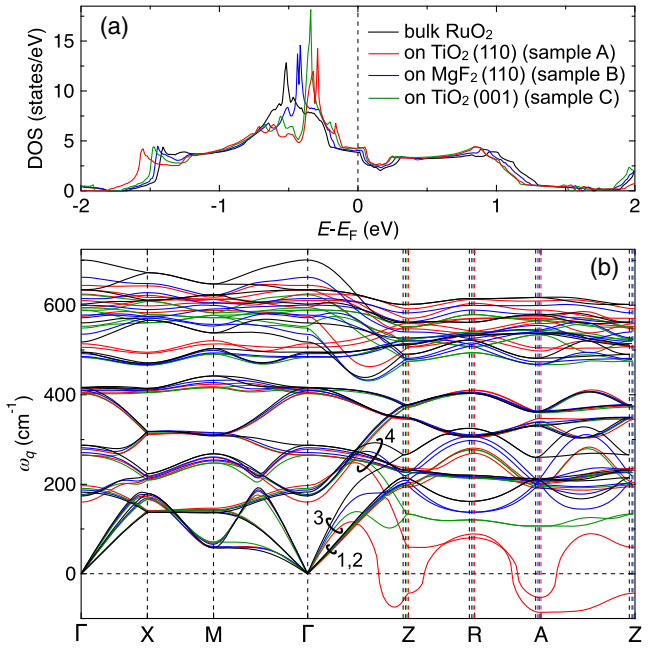

FIG. 4. Electronic and phononic changes in the strained RuO_2 films. (a) Electron density of states calculated for RuO_2 bulk and thin films (samples A, B, and C). (b) Phonon band structures calculated for the same set of samples. In superconducting sample A, acoustic and optical phonon modes oscillating along the c direction (modes 3 and 4) show clear softening, especially around the Z and A points.

oscillating along the c direction (mode 4). Approaching point Z, the c-direction modes 3 and 4 are more complicatedly hybridized with optical modes of O atoms oscillating on the $a-b$ plane. These calculations suggest the possibility that pairing of the Ru $4d$ electrons is mainly mediated by the soft phonon modes induced by the shortening of the c axis or the $M-\mathrm{O}(2)$ bonds. Actually, the Eliashberg spectral function α^2F calculated for the same set of samples shows that the soft phonon modes give a large spectral weight in superconducting sample A, suggesting that the low-frequency part of the soft phonon modes mainly contributes to the superconductivity (for details, see the Supplemental Material [41]).

In summary, we have studied epitaxial strain effect on superconductivity in RuO_2 thin films by combining x-ray diffraction characterization, low-temperature transport measurement, and first-principles calculations for various types of strained films. In particular, a comparison of the (110)-oriented films grown on the TiO_2 and MgF_2 substrates has clarified that shortening of the c axis or the $M-\mathrm{O}(2)$ bonds is essential for emergence of the superconductivity. The theoretical calculations have demonstrated that softening of the two phonon modes oscillating along the c direction is dramatically induced by the lattice parameter change. This Letter suggests that epitaxial strain will become a powerful tool for directly tuning phonon modes and their mediated superconductivity, especially in simple transition metal oxides such as those with a rutile structure, in addition to mechanical pressure [43] and chemical substitution [44,45]. On the other hand, the superconductivity in this system may affected be also by electron correlation or antiferromagnetic ordering, which have not been included in these calculations. We hope that our Letter will trigger further explorations of superconductivity in the simple transition metal oxides by tuning phonon dispersion relations and/or electron phonon interaction through the epitaxial strain.

We would like to thank Y. Tokura and Y. Motome for the fruitful discussions and K. S. Takahashi for experimental advice. This work was supported by Grant-in-Aids for Scientific Research on Innovative Areas No. 19H05825, Scientific Research (S) No. 16H06345, Scientific Research (B) No. JP18H01866, and Early-Career Scientists No. JP19K14654 from MEXT, Japan, by JST PRESTO Grant No. JPMJPR18L2, and by JST CREST Grant No. JPMJCR16F1.

*Corresponding author.
m.uchida@phys.titech.ac.jp

[1] K. H. Bennemann and J. B. Ketterson, *The Physics of Superconductors* (Springer, Berlin, 2003).
[2] N. J. Doyle, J. K. Hulm, C. K. Jones, R. C. Miller, and A. Taylor, Phys. Lett. **26A**, 604 (1968).
[3] J. K. Hulm, C. K. Jones, R. A. Hein, and J. W. Gibson, J. Low Temp. Phys. **7**, 291 (1972).
[4] C. Zhang, F. Hao, G. Gao, X. Liu, C. Ma, Y. Lin, Y. Yin, and X. Li, npj Quantum Mater. **2**, 2 (2017).
[5] K. Yoshimatsu, O. Sakata, and A. Ohtomo, Sci. Rep. **7**, 12544 (2017).
[6] H. Kurokawa, K. Yoshimatsu, O. Sakata, and A. Ohtomo, J. Appl. Phys. **122**, 055302 (2017).
[7] Y. Li *et al.*, NPG Asia Mater. **10**, 522 (2018).
[8] M. K. Forthaus, K. Sengupta, O. Heyer, N. E. Christensen, A. Svane, K. Syassen, D. I. Khomskii, T. Lorenz, and M. M. Abd-Elmeguid, Phys. Rev. Lett. **105**, 157001 (2010).
[9] K. Kaminaga, D. Oka, T. Hasegawa, and T. Fukumura, J. Am. Chem. Soc. **140**, 6754 (2018).
[10] K. Ahadi, L. Galletti, Y. Li, S. Salmani-Rezaie, W. Wu, and S. Stemmer, Sci. Adv. **5**, eaaw0120 (2019).
[11] R. Russell, N. Ratcliff, K. Ahadi, L. Dong, S. Stemmer, and J. W. Harter, Phys. Rev. Mater. **3**, 091401 (2019).
[12] W. D. Ryden, A. W. Lawson, and C. C. Sartain, Phys. Lett. **26A**, 209 (1968).
[13] W. D. Ryden, A. W. Lawson, and C. C. Sartain, Phys. Rev. B **1**, 1494 (1970).
[14] M. Takeuchi, K. Miwada, and H. Nagasaka, Appl. Surf. Sci. **11–12**, 298 (1982).
[15] E. Kolawa, F. C. T. So, W. Flick, X.-A. Zhao, E. T-S. Pan, and M.-A. Nicolet, Thin Solid Films **173**, 217 (1989).

[16] H. Maiwa, N. Ichinose, and K. Okazaki, Jpn. J. Appl. Phys. **33**, 5223 (1994).
[17] J. Si and S. B. Desu, J. Mater. Res. **8**, 2644 (1993).
[18] G. X. Miao, A. Gupta, G. Xiao, and A. Anguelouch, Thin Solid Films **478**, 159 (2005).
[19] J. H. Han, S. W. Lee, S. K. Kim, S. Han, C. S. Hwang, C. Dussarrat, and J. Gatineau, Chem. Mater. **22**, 5700 (2010).
[20] Q. X. Jia, X. D. Wu, S. R. Foltyn, A. T. Findikoglu, and P. Tiwari, Appl. Phys. Lett. **67**, 1677 (1995).
[21] X. Fang, M. Tachiki, and T. Kobayashi, Proc. SPIE Int. Soc. Opt. Eng. **3175**, 331 (1998).
[22] M. Hiratani, Y. Matsui, K. Imagawa, and S. Kimura, Thin Solid Films **366**, 102 (2000).
[23] X. Wang, A. F. Pun, Y. Xin, and J. P. Zheng, Thin Solid Films **510**, 82 (2006).
[24] D.-Y. Kuo, H. Paik, J. N. Nelson, K. M. Shen, D. G. Schlom, and J. Suntivich, J. Chem. Phys. **150**, 041726 (2019).
[25] T. Berlijn, P. C. Snijders, O. Delaire, H.-D. Zhou, T. A. Maier, H.-B. Cao, S.-X. Chi, M. Matsuda, Y. Wang, M. R. Koehler, P. R. C. Kent, and H. H. Weitering, Phys. Rev. Lett. **118**, 077201 (2017).
[26] Z. H. Zhu, J. Strempfer, R. R. Rao, C. A. Occhialini, J. Pelliciari, Y. Choi, T. Kawaguchi, H. You, J. F. Mitchell, Y. Shao-Horn, and R. Comin, Phys. Rev. Lett. **122**, 017202 (2019).
[27] Y. Sun, Y. Zhang, C.-X. Liu, C. Felser, and B. Yan, Phys. Rev. B **95**, 235104 (2017).
[28] M. Uchida and M. Kawasaki, J. Phys. D **51**, 143001 (2018).
[29] J. Ruf, H. Paik, J. Kawasaki, B. Pamuk, H. Nair, N. Schreiber, L. Miao, D. G. Schlom, and K. M. Shen, in *Proceedings of the APS March Meeting, 2019*, Abstract No. R46.00009, https://meetings.aps.org/Meeting/MAR19/Session/R46.9.
[30] M. Uchida, M. Ide, H. Watanabe, K. S. Takahashi, Y. Tokura, and M. Kawasaki, APL Mater. **5**, 106108 (2017).
[31] M. Uchida, M. Ide, M. Kawamura, K. S. Takahashi, Y. Kozuka, Y. Tokura, and M. Kawasaki, Phys. Rev. B **99**, 161111(R) (2019).
[32] M. Uchida, I. Sakuraba, M. Kawamura, M. Ide, K. S. Takahashi, Y. Tokura, and M. Kawasaki, Phys. Rev. B **101**, 035107 (2020).
[33] M. Uchida, W. Sano, K. S. Takahashi, T. Koretsune, Y. Kozuka, R. Arita, Y. Tokura, and M. Kawasaki, Phys. Rev. B **91**, 241119(R) (2015).
[34] J. K. Kawasaki, M. Uchida, H. Paik, D. G. Schlom, and K. M. Shen, Phys. Rev. B **94**, 121104(R) (2016).
[35] P. Giannozzi *et al.*, J. Phys. Condens. Matter **21**, 395502 (2009); **29**, 465901 (2017).
[36] J. P. Perdew, K. Burke, and M. Ernzerhof, Phys. Rev. Lett. **77**, 3865 (1996).
[37] K. F. Garrity, J. W. Bennett, K. M. Rabe, and D. Vanderbilt, Comput. Mater. Sci. **81**, 446 (2014).
[38] S. Baroni, S. de Gironcoli, A. Dal Corso, and P. Giannozzi, Rev. Mod. Phys. **73**, 515 (2001).
[39] Y. Maeno, H. Hashimoto, K. Yoshida, S. Nishizaki, T. Fujita, J. G. Bednorz, and F. Lichtenberg, Nature (London) **372**, 532 (1994).
[40] S. Yonezawa, T. Kajikawa, and Y. Maeno, Phys. Rev. Lett. **110**, 077003 (2013).
[41] See Supplemental Material at http://link.aps.org/supplemental/10.1103/PhysRevLett.125.147001 for more film characterizations and first-principles calculations.
[42] J. H. Xu, T. Jarlborg, and A. J. Freeman, Phys. Rev. B **40**, 7939 (1989).
[43] J. A. Flores-Livas, L. Boeri, A. Sanna, G. Profeta, R. Arita, and M. Eremets, Phys. Rep. **856**, 1 (2020).
[44] K. Kudo, M. Takasuga, Y. Okamoto, Z. Hiroi, and M. Nohara, Phys. Rev. Lett. **109**, 097002 (2012).
[45] B. Wang and K. Ohgushi, J. Phys. Soc. Jpn. **84**, 044707 (2015).